

# CoRe-GS: Coarse-to-Refined Gaussian Splatting with Semantic Object Focus

Hannah Schieber<sup>1</sup>, Dominik Frischmann<sup>1</sup>, Simon Boche<sup>3</sup>, Victor Schaack<sup>1</sup>, Angela Schoellig<sup>2</sup>, Stefan Leutenegger<sup>3</sup> and Daniel Roth<sup>1</sup>

**Abstract**—Mobile reconstruction for autonomous aerial robotics holds strong potential for critical applications such as tele-guidance and disaster response. These tasks demand both accurate 3D reconstruction and fast scene processing. Instead of reconstructing the entire scene in detail, it is often more efficient to focus on specific objects, i.e., points of interest (PoIs). Mobile robots equipped with advanced sensing can usually detect these early during data acquisition or preliminary analysis, reducing the need for full-scene optimization. Gaussian Splatting (GS) has recently shown promise in delivering high-quality novel view synthesis and 3D representation by an incremental learning process. Extending GS with scene editing, semantics adds useful per-splat features to isolate objects effectively.

Semantic 3D Gaussian editing can already be achieved before the full training cycle is completed, reducing the overall training time. Moreover, the semantically relevant area, the PoI, is usually already known during capturing. To balance high-quality reconstruction with reduced training time, we propose CoRe-GS. We first generate a coarse segmentation-ready scene with semantic GS and then refine it for the semantic object using our novel color-based effective filtering for effective object isolation. This is speeding up the training process to be about a quarter less than a full training cycle for semantic GS. We evaluate our approach on two datasets, SCRREAM (real-world, outdoor) and NerDS 360 (synthetic, indoor), showing reduced runtime and higher novel-view-synthesis quality.

## I. INTRODUCTION

Capturing and reconstructing our world is beneficial for a wide range of domains [1], [2], [3], [4], particularly when enhanced beyond traditional 2D imaging. By enabling 3D reconstructions, such captures offer more detailed and explorable scene representations. Applications span aerial imaging [5], medicine [6], [7], cultural heritage preservation and tourism [2], [3], [4], architecture [8], construction [9], planning [10], and robotic manipulation [11], [12], [13]. High-fidelity 3D scene representations are essential for simulation environments, remote mission planning, and robotic navigation, especially in drone- and robot-captured settings. In the context of novel view synthesis (NVS), Gaussian

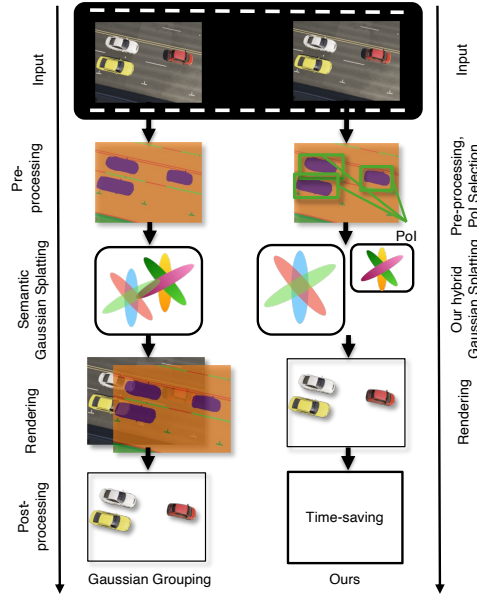


Fig. 1: Comparison of traditional semantic GS following the definition of Ye et al. [15] compared to our approach leveraging directly the knowledge of specific Point of Interests (PoIs) during training time.

Splatting (GS) [14] presents an efficient approach with a trade-off between training time and scene quality.

To further optimize such pipelines, especially in drone-based visual captures, PoI selection can be a valuable strategy to focus on relevant scene areas. A PoI typically guides the camera toward a specific object or region during capture, ensuring that this area is well-represented in the resulting dataset. When constructing 3D representations from these images, PoI metadata can continue to play a role, informing downstream semantic tasks, guiding training prioritization, or supporting scene understanding. While learning-based 3D representations often require significant training overhead, integrating PoI awareness can streamline this process. In particular, semantics tied to PoIs can drive efficient scene representation, offering targeted improvements. Currently, semantic approaches allowing the extraction of PoI objects often suffer from distracting scene parts (floaters) in the filtered scene representation.

For scene refinement, active view selection [16], [17] is a standard methodology. However, these approaches typically optimize the entire scene. Optimizing specific scene parts is

<sup>1</sup>Hannah Schieber, Dominik Frischmann, Victor Schaack, and Daniel Roth are with the Technical University of Munich, Human-Centered Computing and Extended Reality Lab, TUM University Hospital, Clinic for Orthopedics and Sports Orthopedics, Munich Institute of Robotics and Machine Intelligence (MIRMI) hannah.schieber@tum.de, daniel.roth@tum.de

<sup>2</sup>Angela Schoellig is with Technical University of Munich angela.schoellig@tum.de

<sup>3</sup>Simon Boche is with Technical University of Munich simon.boche@tum.de

<sup>2</sup>Stefan Leutenegger is with the Mobile Robotics Lab, Department of Mechanical and Process Engineering, ETH Zurich lestefan@ethz.ch

usually not applied, and post-processing approaches suffer from outliers (floaters) [4], [18], [15]. Optimizing specific scene parts can be acquired with semantics, but incorporating semantic segmentation often introduces additional computational overhead. Although semantic GS offers sufficient fidelity to support selective refinement of drone-captured regions, it is generally applied to the whole scene [4], [15]. This extends the overall runtime for initial reconstruction.

To address this challenge, we propose a refinement of PoIs in GS. Our method reduces training time for high-quality scene reconstruction by focusing on a single PoI. We extend classical and semantic GS by integrating PoI extraction, accelerating the overall training process. Once a segmentation-ready scene (coarse scene) is created, further processing refines only the extracted object, the PoI, in roughly a quarter of the time required by standard semantic GS [15]. By effectively mitigating color space discrepancies during PoI refinement, our approach enhances the visual quality of the resulting scenes. We demonstrate our method in both indoor and outdoor settings using scenes from the SCREAM [19] and NeRDS 360 [20] datasets.

To summarize, we contribute:

- A PoI refinement for an efficient and more accurate editable GS.
- A color-based effective filtering method, for GS PoI refinement.
- A comprehensive evaluation on diverse datasets, testing our approach on both indoor and outdoor scenes with different PoI sizes to assess adaptability.

## II. RELATED WORK

Our approach targets editable radiance fields and reduces the overall training time to extract PoIs from these radiance field representations. Therefore, we provide an overview of state-of-the-art editing of radiance fields, refinement, and semantics.

### A. 3D Scene Refinement

Various strategies exist for scene refinement. A naive but straightforward approach is to capture more images, while more advanced methods target selective views [17], path trajectory planning [21], [22], or a combination of both [16].

While enhancing the visual quality of the scene representation is one approach, Peralta et al. [21] focus on adapting the capturing path. Similarly, Chen et al. [22] introduce GenNBV, which optimizes drone camera paths using reinforcement learning. While these approaches apply to a broader scope, others directly target GS optimization. Aside from optimizing the capturing path, in already captured scenes, FisherRF [17] applies uncertainty quantification to select ideal views within GS. Lit et al. [16] leverages efficient viewpoint sampling and path planning combined with a dense scene representation via GS.

Refinement of the scene based on semantic PoI offers a different solution to the problem, as the complete scene does not need to be refined.

### B. Semantic and Language-Guided Radiance Fields

Editable radiance fields often employ semantics or language guidance to adapt the final scene representation [23], [15], [4], [24], [25], [26]. Different final applications can be considered, ranging from object removal to search until object extraction.

1) *Object Removal*: Although GS [14], now dominates radiance fields, its predecessor, neural radiance fields (NeRF) [27], [28], already presented editable approaches [29], [28]. Inpainting can be used to remove objects from the initial scene or from the learned scene representation [30], [31], [32] with the goal to keep an accurate geometry of the scene. Yin et al. [30] leveraged SAM [33] and with LaMa [34] to inpaint selected objects within a NeRF. In a similar approach, Weder et al. [31] proposed an inpainting-based NeRF solution designed to remove unwanted objects. Similarly, GS has been addressing object removal tasks using segmentation masks first of the unwanted object [32]. For GS, Huang et al. address this with SAM masks and depth-guided inpainting.

Many GS approaches allow object removal [23], [15] and, combined with an additional inpainting model like LaMa [34], also enable inpainted Gaussians.

2) *Semantic Search and Editing*: While NeRF already showed great potential, GS [14] offers better rendering capability and adaptability, due to its explicit scene representation. Its real-time rendering capability is especially beneficial for scene exploration. Often, multiple models are combined. Yu et al. [25] leverage CLIP, Droid-SLAM [35], and GS for robotic navigation. In addition to language guidance, HAMMER [36] produces semantic GS maps from multiple input devices, such as robots and smart glasses, allowing direct editing of the resulting scene representations.

Similarly, Qu et al. [37] proposed a point-based editing approach that enables manipulation of Gaussians directly within the scene. Furthermore, segmentation-based GS allows scene editing per class, often proposed as a downstream task [23], [15]. Ye et al. [15] proposed segmentation-based grouping, with the so-called Gaussian Grouping (GG), extending the Gaussian representation with a feature field for classifier-based segmentation. Moreover, they demonstrated scene editing, such as inpainting and object removal, as a downstream task. Within GAGA [23], Lyu et al. [23] proposed segmentation-based GS using a memory bank. Although segmentation quality can be improved with GAGA, training time also increases, as the approach uses pure GS [14] as input, followed by several semantic training and label preparation steps.

While many approaches [15], [23] leverage foundation models [38], [33] for segmentation ground truth, Schieber et al. [4] use a supervised approach, effectively removing large object parts in outdoor scenes. While it is promising for large objects, foundation models have broader scalability to unknown classes.

### C. Applied Editable Radiance Fields

Adding semantic segmentation to the radiance field representation provides the opportunity to later edit the explicit GS scene representation. Many works [23], [15], [4], demonstrate this ability in a post-processing step, others directly integrate it into applications. Li et al. [11] added semantics for robotic manipulation for a limited number of views. They address language-guided grasping. Another grasping solution is proposed by Ji et al. [12]. They leverage GS, MobileSAM, and CLIP to propose potential object grasp positions.

### D. Research Gap

While scene editing [15], [4], [26], path planning [21], [22], and camera view selection [17] are widely explored, optimizing the semantic representations used within these contexts can still be optimized. Complete semantic training is costly, and post-processing PoI extraction suffers from inconsistency (floaters). To address these challenges, we propose PoI refinement GS, where a coarse semantic GS provides initial scene understanding and PoI are selectively refined, achieving high quality with reduced training time.

## III. METHOD

### A. Gaussian Segmentation and Point-of-Interest Extraction

We apply the training process of semantic GS [15] for 3k iterations and obtain a coarse scene representation, see Figure 2. The pre-segmentation step used enables each part of the scene to be represented by a semantic class or instance class, depending on the given database. Using the assigned class ID, a filtering step is performed to extract the PoI.

During the pre-extraction phase, the PoI is selected based on its class ID, such as the class “car”, see Figure 2. The images are filtered on the basis of the presence of this class. The Gaussians are then filtered accordingly, preserving only those that predominantly belong to the selected PoI.

For each retained image, binary masks ( $M$ ) are generated to isolate the target object: for each pixel  $(u, v)$  corresponding to the segmentation class are assigned a value of 1 is assigned, while all other pixels are set to 0:

$$M(u, v) = \begin{cases} 1, & \text{if } (u, v) \text{ belongs to the target object ID} \\ 0, & \text{otherwise} \end{cases} \quad (1)$$

These binary masks ( $M$ ) are used to effectively remove additional information. This is required in the later refinement process to ensure that only the relevant parts of the scene within the PoI are processed in the refinement step.

In addition, the color distribution of the image is analyzed for each selected image to determine the most pronounced color in the image in relation to the other colors in the image. To speed up this process, the images are downscaled by a factor of 0.5. Unique colors are then extracted from the downscaled images, and a KD-tree is created based on these colors. The set of existing image colors is given by:

$$C = \{c_i\}_{i=1}^N, \quad \text{where } c_i \in [0, 1]^3 \in \mathbb{R} \quad (2)$$

A predefined reduced RGB color space ( $P$ ):

$$P = \{p_j\}_{j=1}^J, \quad \text{where } p_j \in [0, 1]^3 \in \mathbb{R} \quad (3)$$

is sampled systematically across the RGB spectrum  $(r, g, b)$ .  $P$  is queried against the constructed KD-tree. The color with the greatest minimum Euclidean distance ( $\|p_j - c_i\|_2$ ) from all existing image colors is identified as the “furthest” color:

$$p^* = \arg \max_{p_j \in P} \left( \min_{c_i \in C} \|p_j - c_i\|_2 \right) \quad (4)$$

where the Euclidean distance in RGB space is given by:

$$\|p_j - c_i\|_2 = \sqrt{(r_{p_j} - r_{c_i})^2 + (g_{p_j} - g_{c_i})^2 + (b_{p_j} - b_{c_i})^2} \quad (5)$$

where  $r, g$ , and  $b$  represent the RGB values normalized to the interval  $[0, 1]$ . This furthest color ( $p^*$ ), along with its corresponding maximum minimum distance value, is recorded for each image. These results are subsequently saved for analysis and utilized during the refinement process.

### B. Point of Interest Refinement

Based on extracted colors, the frequency of the most common color is analyzed. The most frequent color is used as the universal background for the subsequent rendering. To focus refinement on the selected PoI, the training images and loss calculations are masked with binary masks  $M(x, y)$ .

We initialize our GS using the filtered points of the PoI and start the training process for the remaining 27k iterations. Additionally, our GS is periodically filtered to eliminate potential artifacts during refinement.

1) *Periodic Scene Filtering*: While segmentation classes can initially be utilized for isolating the PoI due to the semantic information provided by any 3D semantic GS, such segmentation or instance classes are not leveraged during the refinement step, as the semantic rasterizer and classifier lead to an increase in training time. Instead, we employ our color-based filtering strategy for additional pruning and adjustment of the PoI GS during refinement. In the pre-extraction step, we received the most distinct (“furthest”) color ( $p^*$ ) relative to the colors already present, measured by Euclidean distance in RGB color space.

Using  $p^*$ , we effectively filter out unwanted Gaussians. Given the substantial color difference between  $p^*$  and meaningful Gaussians, unwanted artifacts can be identified and removed through color-based filtering. Specifically, for each view, the color of each Gaussian is computed by evaluating its spherical harmonics (SH) coefficients relative to the camera’s viewing direction. The resulting RGB color is then compared to the previously identified  $p^*$ . The Euclidean distance between the Gaussians computed RGB color and  $p^*$  is calculated. If this distance falls below a threshold, the Gaussian is considered an artifact and marked for removal. All Gaussians identified as artifacts based on this criterion are pruned from the scene representation, thereby significantly reducing unwanted visual artifacts that typically manifest

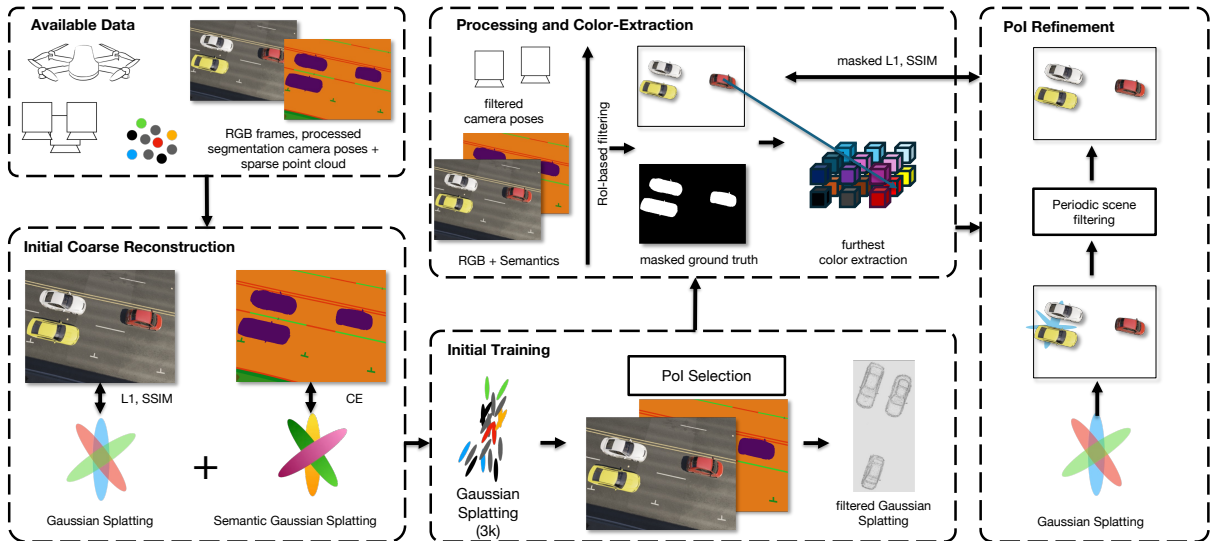


Fig. 2: **Our approach.** Our approach first trains a semantic GS scene representation (left) [15] for a set of initial iterations (3k). Followed by that, the PoI is extracted based on the given segmentation class from the semantic GS (center). Based on the segmentation class ID, we extract only the Gaussians per PoI. In a last step, the PoI is refined using our periodic scene filtering with the previously extracted furthest color.

around object boundaries. Given the average distance  $d_{avg}$  computed earlier from the  $p^*$  selection process, the Gaussians selected for removal at a removal iteration are those satisfying:

$$G_{\text{remove}} = \{G_i \mid d(c_{G_i}, c_{bg}) < d_{\text{remove}}\} \quad (6)$$

The removal distance is defined as:

$$d_{\text{remove}} = t_r \cdot d_{\text{avg}} \quad (7)$$

The removal threshold defaults to  $t_r = 0.5$ . This process ensures that the refinement specifically targets meaningful regions and maintains clean, artifact-free reconstructions throughout iterative refinement.

### C. Gaussian Rasterization

Our rasterization process consists of two key stages. First, we build upon semantic GS. This initialization and pre-training phase enables the model to distinguish and categorize scene elements effectively, leveraging semantic information for a strong foundation in subsequent refinements.

In the main phase of our approach, which focuses on PoI refinement, we utilize the standard GS rasterizer while employing optimizations to enhance efficiency. Specifically, we accelerate the training process using a fused-SSIM loss function alongside a sparse Adam optimizer, significantly improving convergence speed [14]. Additionally, we integrate our PoI masking mechanism, allowing for targeted refinement of relevant regions while optimizing a clean scene representation and loss computation. This selective approach ensures that our approach concentrates on relevant areas.

## IV. EVALUATION

### A. Metrics

To evaluate the rendering quality of our approach, we use the metrics peak signal-to-noise ratio (PSNR) and similarity index measure (SSIM) [39]. For the update time, we specify the total training time in (s) and iterations per second (*it/s*). In Table I and Table II, differences in PSNR are marked as:  $1\pm$ ,  $-1.0$ , and  $\leq 1.0$ . For time in seconds we mark the lowest values within  $\pm 30$  seconds, values larger but below  $\geq 100$  seconds,  $> 100$  and  $< 1000$  seconds, and values  $1000 > \text{seconds}$ . The best values per metric are marked in **bold**.

### B. Implementation Details

a) *Hardware Setup:* Our approach and the comparison methods (pure GS [14] and GG [15]) are implemented in Python with PyTorch and CUDA. All scenes were evaluated on desktop PCs with an RTX3090 with 24 GB VRAM.

b) *Periodic Scene Filtering:* We use parallelization to calculate  $p^*$ . For this we use a thread pool with  $N$  workers so that several views can be processed simultaneously. To maintain visual fidelity during the refinement process, periodic filtering of the Gaussian based on color similarity is performed every 1000 training iterations.

### C. Datasets

a) *NeRDS 360 [20]:* We use the COLMAP subset from the NeRDS 360 dataset [20]. The scenes are particularly interesting as they show urban landscapes and vehicles that resemble the conditions of possible rescue situations and offer a  $360^\circ$  view of a street scene. The respective scenes with COLMAP ground truth are two from *SF\_VanNessAveAndTurkSt* (3,5), the scenes 1, 2, and 3 from

TABLE I: **Evaluation on NeRDS 360 [20]**. We report PSNR, SSIM, and Time in seconds. We compare GG with a convex-hull removal and GG with a direct removal scheme with our method.

Scene	GG [15] (convex-hull)			GG [15] (direct removal)			Ours		
	PSNR↑	SSIM↑	Time↓	PSNR↑	SSIM↑	Time↓	PSNR↑	SSIM↑	Time↓
6thAndMission_medium									
6	11.403	0.724	2560	16.662	0.828	2560	<b>26.430</b>	<b>0.962</b>	<b>418</b>
7	11.403	0.724	1957	21.726	0.904	1957	<b>28.106</b>	<b>0.968</b>	<b>469</b>
10	11.117	0.688	2061	22.378	0.896	2061	<b>27.466</b>	<b>0.964</b>	<b>447</b>
GrantAndCalifornia									
1	9.729	<b>0.753</b>	1848	20.036	0.885	1848	<b>25.989</b>	<b>0.959</b>	<b>446</b>
2	9.479	0.703	2005	19.371	0.879	2005	26.876	0.959	<b>446</b>
3	9.701	0.744	1867	18.096	0.853	1867	<b>28.053</b>	<b>0.965</b>	<b>443</b>
VanNessAveAndTurkSt									
3	12.276	0.788	1939	17.802	0.852	1939	<b>26.197</b>	<b>0.957</b>	<b>464</b>
5	11.097	0.753	2160	19.040	0.865	2160	<b>28.518</b>	0.974	<b>480</b>
Mean	11.238	0.748	2050	19.389	0.870	2050	<b>27.204</b>	<b>0.963</b>	<b>460</b>

TABLE II: **Evaluation on SCRREAM [19]**. For all scenes, we use the full configuration (.full\_00). We report PSNR, SSIM, and Time in seconds. As a comparison method, we choose GG with a direct object removal.

Scene	GG [15]			Ours		
	PSNR↑	SSIM↑	Time	PSNR↑	SSIM↑	Time
scene01	<b>31.90</b>	<b>0.927</b>	2614	30.89	0.903	<b>709</b>
scene02	25.61	<b>0.849</b>	2766	<b>25.97</b>	0.792	<b>1083</b>
scene03	<b>36.52</b>	<b>0.965</b>	2645	35.79	0.954	<b>656</b>
Mean	<b>31.34</b>	<b>0.914</b>	2675	30.88	0.883	<b>816</b>

TABLE III: **Comparison of our approach with different initialization iterations**. We evaluated after 7k and 30k iterations on scene SF\_6thAndMission\_medium10 [20]. We marked the best approach **bold**. We report PSNR, SSIM and Time in seconds.

initial iterations	7k iterations			30k iterations		
	PSNR↑	SSIM↑	Time↓	PSNR↑	SSIM↑	Time↓
1000	26.628	0.958	<b>114</b>	27.107	0.962	380
2000	27.054	0.961	140	27.542	0.965	391
3000	27.105	<b>0.962</b>	180	<b>27.668</b>	<b>0.965</b>	447
4000	<b>27.117</b>	<b>0.962</b>	224	27.553	0.964	480

SF\_GrantAndCalifornia, and three scenes from 6th and Mission (6, 7, 10). As PoI we defined the class “car”.

b) *SCRREAM [19]*: For an indoor proof of concept, we evaluated our approach on SCRREAM [19]. Each scene contains separate recordings with a variety of objects. For our comparison we use *Scene01*, *Scene02*, and *Scene03* all in the setting *full*. We use the class *chair* as PoI.

#### D. Baselines

For the comparison, we selected GG [15], as it is the state-of-the-art in GS separation and showed the same performance in NVS as traditional GS.

#### E. Novel View Synthesis Quality

We compare the overall performance on all datasets with a focus on our speedup compared to semantic GS, evaluate the used initialization iterations using both baselines, and compare our approach to traditional GS in terms of NVS and runtime.

1) *Comparison to Full Semantic Gaussian Splatting*: Since our method leverages semantic GS for initialization, we compare it with the respective method, using the complete training cycle.

With regard to the quality of NVS, we focus on PSNR and SSIM, where PoI masking can be applied. This ensures a fair comparison when calculating these metrics. As shown in Table I, our approach outperforms GG in three scenes while achieving competitive results overall in terms of SSIM. For PSNR, both methods show similar ranges, approximately  $\pm 0.5$ . However, our approach not only achieves this level of performance but also demonstrates a significantly reduced training time, particularly excelling in performance for the “car” class.

To evaluate our approach in multiple settings, we also compared it in an indoor dataset. The SCRREAM dataset [19] (real-world, indoor) consists of diverse scenes with highly accurate ground truth for semantic segmentation. As shown in Table II, our approach outperforms GG in PSNR on one scene and remains competitive across all three scenes in both PSNR and SSIM. As shown in Figure 5, no visual downside is visible for our approach; rather, we show clearer boundaries.

In Figure 3, we provide a direct comparison of filtered outputs between GG and our method. A comparison of our PoI approach with GG using convex hull removal reveals that the convex hull method retains numerous outliers (floaters) from the original scene. Similarly, when using non-convex, class-based removal, additional outliers become evident, as shown in Figure 3. Despite these differences, our method exhibits no significant drawbacks in terms of NVS quality.

2) *Impact of Varying Numbers Initialization Iterations*: For the initialization, we analyzed the trade-off between creating a visually explorable scene and minimizing training time. We evaluated subjective visual quality as shown in Figure 4, and objective metric-based results, see Table III.

The visual quality shows that using a low-quality semantic GS scene for initialization can reduce the final quality within a range of  $\pm 0.5$ . Although this difference is per se not high, when looking at Figure 4 for a visual scene exploration, more iterations are beneficial. 3000 to 4000 iterations show clearer

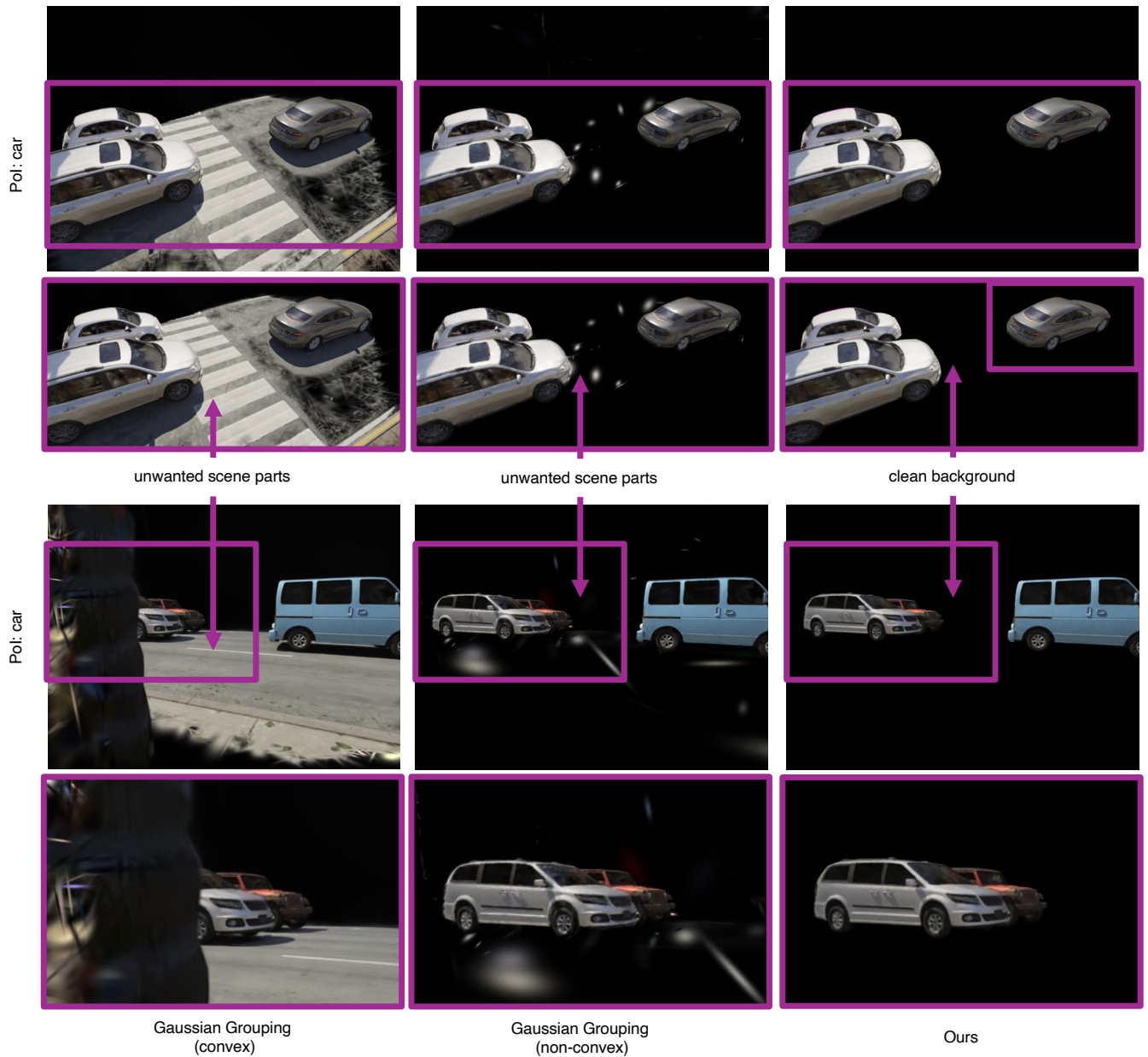


Fig. 3: Exemplary occlusion removal comparison on the scenes *SF\_GrantAndCalifornia1* (bottom) *SF\_6thAndMission\_medium10* (top) after 30,000 iterations. Post-training isolation using Gaussian Grouping (b, c) partially recovers occlusions, with convex hull usage influencing the result.



Fig. 4: Initialization example on *SF\_6thAndMission\_medium10* from the Neo360 dataset [20]. The rendering iteration is denoted among each column.



(a) GG convex (b) GG non-convex (c) Ours

Fig. 5: **SCRREAM scene01 after 30k iterations (images cropped to PoI)**. GG using a convex hull (a), and GG using a non-convex hull (b), and our PoI refinement (c).

TABLE IV: **Comparison of GS after 15k and 30k training iterations**. We mask PSNR and SSIM with the GT object mask of the car, as GS does not offer per-object extraction. We report the best result in **bold**.

	Iterations	PSNR $\uparrow$	SSIM $\uparrow$	TIME [s] $\downarrow$
GS	30000	21.40	<b>0.862</b>	417
Ours	15000	<b>21.73</b>	0.859	<b>285</b>

results. Thus, 3000 iterations provide a positive balance between training time and PSNR and SSIM result.

3) *Comparison to Traditional Gaussian Splatting*: Traditional GS [14] has seen significant improvements, including a reduction in training time. However, while segmentation-based removal is not possible in traditional GS, it is possible to mask the metric calculation for a comparison in quality. When comparing this method with our approach, see Table IV, we demonstrate that our hybrid scene representation, initialized with semantic GS, outperforms traditional GS in both runtime and PSNR. For this comparison, we used masked PSNR and masked SSIM as traditional GS does not allow the removal of specific scene objects. Our approach achieves a better PSNR in just half the number of training iterations, while SSIM is almost the same performance.

#### F. Speedup Comparison

Adding segmentation to the GS rasterization process can enhance quality, but also increases the training time. As shown in Table I, GG around 2050 seconds to process all scenes compared to our approach, which requires 460 seconds. Our approach only requires a segmentation and a ready-to-explore scene (3k), and we achieve a maximum training time of around 460 seconds, where around 120 seconds can be attributed to the initialization training and around 4 seconds to the PoI extraction. This shows that our approach reduced the training load enormously.

## V. DISCUSSION

We propose a novel approach for PoI in GS, leveraging semantic GS [15] in the first stage to initialize the PoI refinement step. The semantic GS module is interchangeable and independent from the PoI refinement, fostering modularity and extendability of the approach. Our masking and PoI selection allow for an efficient training cycle. The PoI selection ensures that only relevant data for the target object or target area contributes to the scene optimization, which allows a more focused and faster training.

As shown in Table I, the runtime of GG is notably higher compared to our approach. While semantic information is necessary for selecting one PoI or multiple PoIs after obtaining the rough scene representation, our method provides a substantial speedup, performing faster than training full GG and extracting more visually appealing PoIs (Figure 3).

Experiments on the SCRREAM dataset validate the robustness of our method in different environments. While its relative advantage over the baselines is slightly smaller compared to the outdoor NeRDS 360 scenes, our method still produces strong results.

Moreover, the PoI refinement gives an advantage for occluded areas, while in the full scene, a pole or street light could occlude the PoI from different NVS perspectives. Selecting a PoI and extracting it shows the advantage of our approach against occlusion. This capability offers a more complete understanding of the object’s geometry and structure from the same perspective, a feature not achievable with GG.

## VI. LIMITATIONS

Our approach relies on high-quality segmentation, and its effectiveness may be constrained when segmentation accuracy is insufficient. Previous work [4] has already demonstrated the critical role of segmentation labels in GS-based methods, highlighting their impact on reconstruction quality and downstream tasks.

## VII. CONCLUSION

In summary, we introduce a PoI refinement framework for GS that selectively enhances segmentation-based regions critical for scene exploration. By focusing computation on targeted scene areas, our approach produces higher-fidelity, PoI without the overhead of refining the entire scene representation. Our evaluation on two benchmarks demonstrates clear advantages over both standard GS and semantic GS. Unlike standard GS, which lacks PoI support, our method achieves targeted visual refinement, and compared to semantic GS, it reduces training time while preserving segmentation accuracy and rendering quality. These results highlight our approach’s efficiency and visual quality.

## ACKNOWLEDGMENTS

This work has been partially supported by the Technical University of Munich, Munich, Germany, within its MIRMI seed fund scheme.

## REFERENCES

- [1] H. Li, F. Deuser, W. Yin, X. Luo, P. Walther, G. Mai, W. Huang, and M. Werner, "Cross-view geolocalization and disaster mapping with street-view and VHR satellite imagery: A case study of hurricane IAN," *ISPRS Journal of Photogrammetry and Remote Sensing*, vol. 220, pp. 841–854, 2025, publisher: Elsevier.
- [2] L. Gomes, O. R. P. Bellon, and L. Silva, "3d reconstruction methods for digital preservation of cultural heritage: A survey," *Pattern Recognition Letters*, vol. 50, pp. 3–14, 2014, publisher: Elsevier.
- [3] T. Hasselman, W. H. Lo, T. Langlotz, and S. Zollmann, "ARephotography: Revisiting historical photographs using augmented reality," in *Extended Abstracts of the 2023 CHI Conference on Human Factors in Computing Systems*, 2023, pp. 1–7.
- [4] H. Schieber, J. Young, T. Langlotz, S. Zollmann, and D. Roth, "Semantics-controlled gaussian splatting for outdoor scene reconstruction and rendering in virtual reality," in *2025 IEEE Conference Virtual Reality and 3D User Interfaces (VR)*. IEEE, 2025, pp. 318–328.
- [5] J. Tang, Y. Gao, D. Yang, L. Yan, Y. Yue, and Y. Yang, "DroneSplat: 3d gaussian splatting for robust 3d reconstruction from in-the-wild drone imagery," in *Proceedings of the Computer Vision and Pattern Recognition Conference (CVPR)*, 2025, pp. 833–843.
- [6] K. Yu, A. Winkler, F. Pankratz, M. Lazarovici, D. Wilhelm, U. Eck, D. Roth, and N. Navab, "Magnoramas: Magnifying dioramas for precise annotations in asymmetric 3d teleconsultation," in *2021 IEEE Virtual Reality and 3D User Interfaces (VR)*. IEEE, 2021, pp. 392–401.
- [7] C. Kleinbeck, H. Schieber, K. Engel, R. Gutjahr, and D. Roth, "Multi-layer gaussian splatting for immersive anatomy visualization," *IEEE Transactions on Visualization and Computer Graphics*, 2025, publisher: IEEE.
- [8] Z. Cai, J. Yang, T. Wang, H. Huang, and Y. Guo, "3d reconstruction of buildings based on 3d gaussian splatting," *The International Archives of the Photogrammetry, Remote Sensing and Spatial Information Sciences*, vol. 48, pp. 37–43, 2024, publisher: Copernicus GmbH.
- [9] S. Rüter, K. Waldow, N. Bartels, and A. Fuhrmann, "3d gaussian splatting for construction sites," in *24th International Conference on Construction Applications of Virtual Reality (CONVR 2024)*, vol. 11, 2024.
- [10] C. Kleinbeck, H. Zhang, B. D. Killeen, D. Roth, and M. Unberath, "Neural digital twins: reconstructing complex medical environments for spatial planning in virtual reality," *International Journal of Computer Assisted Radiology and Surgery*, pp. 1–12, 2024.
- [11] Y. Li and D. Pathak, "Object-aware gaussian splatting for robotic manipulation," in *ICRA 2024 Workshop on 3D Visual Representations for Robot Manipulation*, 2024.
- [12] M. Ji, R.-Z. Qiu, X. Zou, and X. Wang, "Graspsplats: Efficient manipulation with 3d feature splatting," 2024.
- [13] J. Yu, K. Hari, K. El-Refai, A. Dalal, J. Kerr, C. M. Kim, R. Cheng, M. Z. Irshad, and K. Goldberg, "Persistent object gaussian splat (POGS) for tracking human and robot manipulation of irregularly shaped objects," 2025. [Online]. Available: <https://arxiv.org/abs/2503.05189>
- [14] B. Kerbl, G. Kopanas, T. Leimkühler, and G. Drettakis, "3d gaussian splatting for real-time radiance field rendering," *ACM Transactions on Graphics*, vol. 42, no. 4, pp. 1–14, 2023, publisher: ACM.
- [15] M. Ye, M. Danelljan, F. Yu, and L. Ke, "Gaussian grouping: Segment and edit anything in 3d scenes," in *European Conference on Computer Vision*. Springer, 2024, pp. 162–179.
- [16] Y. Li, Z. Kuang, T. Li, Q. Hao, Z. Yan, G. Zhou, and S. Zhang, "Activesplat: High-fidelity scene reconstruction through active gaussian splatting," *IEEE Robotics and Automation Letters*, 2025, publisher: IEEE.
- [17] W. Jiang, B. Lei, and K. Daniilidis, "Fisherrf: Active view selection and uncertainty quantification for radiance fields using fisher information," 2023.
- [18] X. Hu, Y. Wang, L. Fan, J. Fan, J. Peng, Z. Lei, Q. Li, and Z. Zhang, "SAGD: Boundary-enhanced segment anything in 3d gaussian via gaussian decomposition," *arXiv preprint arXiv:2401.17857*, 2024.
- [19] H. Jung, W. Li, S.-C. Wu, W. Bittner, N. Brasch, J. Song, E. Pérez-Pellitero, Z. Zhang, A. Moreau, N. Navab, and others, "SCRREAM: SCan, register, REnd and map: A framework for annotating accurate and dense 3d indoor scenes with a benchmark," *Advances in Neural Information Processing Systems*, vol. 37, pp. 44 164–44 176, 2025.
- [20] M. Z. Irshad, S. Zakharov, K. Liu, V. Guizilini, T. Kollar, A. Gaidon, Z. Kira, and R. Ambrus, "Neo 360: Neural fields for sparse view synthesis of outdoor scenes," in *Proceedings of the IEEE/CVF International Conference on Computer Vision*, 2023, pp. 9187–9198.
- [21] D. Peralta, J. Casimiro, A. M. Nilles, J. A. Aguilar, R. Atienza, and R. Cajote, "Next-best view policy for 3d reconstruction," in *European Conference on Computer Vision*. Springer, 2020, pp. 558–573.
- [22] X. Chen, Q. Li, T. Wang, T. Xue, and J. Pang, "Gennbv: Generalizable next-best-view policy for active 3d reconstruction," in *Proceedings of the IEEE/CVF Conference on Computer Vision and Pattern Recognition*, 2024, pp. 16 436–16 445.
- [23] W. Lyu, X. Li, A. Kundu, Y.-H. Tsai, and M.-H. Yang, "Gaga: Group any gaussians via 3d-aware memory bank," 2024, eprint: 2404.07977.
- [24] J. Kerr, C. M. Kim, K. Goldberg, A. Kanazawa, and M. Tancik, "Lerf: Language embedded radiance fields," in *Proceedings of the IEEE/CVF International Conference on Computer Vision*, 2023, pp. 19 729–19 739.
- [25] J. Yu, K. Hari, K. Srinivas, K. El-Refai, A. Rashid, C. M. Kim, J. Kerr, R. Cheng, M. Z. Irshad, A. Balakrishna, and others, "Language-embedded gaussian splats (legs): Incrementally building room-scale representations with a mobile robot," in *2024 IEEE/RSJ International Conference on Intelligent Robots and Systems (IROS)*. IEEE, 2024, pp. 13 326–13 332.
- [26] Q. Zhang, Y. Xu, C. Wang, H.-Y. Lee, G. Wetzstein, B. Zhou, and C. Yang, "3ditscene: Editing any scene via language-guided disentangled gaussian splatting," 2024.
- [27] B. Mildenhall, P. P. Srinivasan, M. Tancik, J. T. Barron, R. Ramamoorthi, and R. Ng, "NeRF: Representing scenes as neural radiance fields for view synthesis," in *European Conference on Computer Vision (ECCV)*, 2020, pp. 405–421.
- [28] M. Z. Irshad, M. Comi, Y.-C. Lin, N. Heppert, A. Valada, R. Ambrus, Z. Kira, and J. Tremblay, "Neural fields in robotics: A survey," 2024, eprint: 2410.20220. [Online]. Available: <https://arxiv.org/abs/2410.20220>
- [29] C. Wang, M. Chai, M. He, D. Chen, and J. Liao, "Clip-nerf: Text-and-image driven manipulation of neural radiance fields," in *Proceedings of the IEEE/CVF Conference on Computer Vision and Pattern Recognition*, 2022, pp. 3835–3844.
- [30] Y. Yin, Z. Fu, F. Yang, and G. Lin, "Or-nerf: Object removing from 3d scenes guided by multiview segmentation with neural radiance fields," 2023.
- [31] S. Weder, G. Garcia-Hernando, A. Monszpart, M. Pollefeys, G. J. Brostow, M. Firman, and S. Vicente, "Removing objects from neural radiance fields," in *Proceedings of the IEEE/CVF Conference on Computer Vision and Pattern Recognition (CVPR)*, 2023-06, pp. 16 528–16 538.
- [32] S.-Y. Huang, Z.-T. Chou, and Y.-C. F. Wang, "3d gaussian inpainting with depth-guided cross-view consistency," in *Proceedings of the Computer Vision and Pattern Recognition Conference*, pp. 26 704–26 713.
- [33] A. Kirillov, E. Mintun, N. Ravi, H. Mao, C. Rolland, L. Gustafson, T. Xiao, S. Whitehead, A. C. Berg, W.-Y. Lo *et al.*, "Segment anything," pp. 4015–4026, 2023.
- [34] R. Suvorov, E. Logacheva, A. Mashikhin, A. Remizova, A. Ashukha, A. Silvestrov, N. Kong, H. Goka, K. Park, and V. Lempitsky, "Resolution-robust large mask inpainting with fourier convolutions," in *Proceedings of the IEEE/CVF winter conference on applications of computer vision*, 2022, pp. 2149–2159.
- [35] Z. Teed and J. Deng, "Droid-slam: Deep visual slam for monocular, stereo, and rgb-d cameras," *Advances in neural information processing systems*, vol. 34, pp. 16 558–16 569, 2021.
- [36] J. Yu, T. Chen, and M. Schwager, "HAMMER: Heterogeneous, multi-robot semantic gaussian splatting," *IEEE Robotics and Automation Letters*, 2025, publisher: IEEE.
- [37] Y. Qu, D. Chen, X. Li, X. Li, S. Zhang, L. Cao, and R. Ji, "Drag your gaussian: Effective drag-based editing with score distillation for 3d gaussian splatting," 2025.
- [38] H. K. Cheng, S. W. Oh, B. Price, A. Schwing, and J.-Y. Lee, "Tracking anything with decoupled video segmentation," in *Proceedings of the IEEE/CVF International Conference on Computer Vision*, 2023, pp. 1316–1326.
- [39] Z. Wang, A. C. Bovik, H. R. Sheikh, and E. P. Simoncelli, "Image quality assessment: from error visibility to structural similarity," *IEEE transactions on image processing*, vol. 13, no. 4, pp. 600–612, 2004.